

Combined overexpression of ATXN1L and mutant ATXN1 knockdown by AAV rescue motor phenotypes and gene signatures in SCA1 mice

Ellie M. Carrell,¹ Megan S. Keiser,¹ Ashley B. Robbins,^{1,2} and Beverly L. Davidson^{1,3}

¹Raymond G. Perelman Center for Cellular and Molecular Therapeutics, The Children's Hospital of Philadelphia, 6400 Colket Translational Research Building, 3501 Civic Center Boulevard, Philadelphia, PA 19104, USA; ²Department of Neuroscience, Biomedical Graduate Studies Program, University of Pennsylvania, Philadelphia, PA, 19104 USA; ³Department of Pathology & Laboratory Medicine, University of Pennsylvania, Philadelphia, PA, 19104 USA

Spinocerebellar ataxia type 1 (SCA1) is an autosomal dominant neurodegenerative disease caused by a (CAG) repeat expansion in the coding sequence of ATXN1. The primary mechanism of disease in SCA1 is toxic gain of function by polyglutamine-expanded mutant ATXN1 and is compounded by partial loss of wild-type function. Addressing both disease mechanisms, we have shown that virally expressed RNA interference targeting ATXN1 can both prevent and reverse disease phenotypes in SCA1 mice, and that overexpression of the ATXN1 homolog, ataxin 1-like (ATXN1L), improves disease readouts when delivered pre-symptomatically. Here, we combined these therapeutic approaches into two, dual component recombinant adeno-associated virus (rAAV) vectors and tested their ability to reverse disease in symptomatic SCA1 mice using behavior, pathological, and next-generation sequencing assays. Mice treated with vectors expressing human ATXN1L (hATXN1L) alone showed motor improvements and changes in gene expression that reflected increases in pro-development pathways. When hATN1L was combined with miS1, a previously validated microRNA targeting *hATXN1*, there was added normalization of disease allele-induced changes in gene expression along with motor improvements. Our data show the additive nature of this two-component approach for a more effective SCA1 therapy.

INTRODUCTION

Spinocerebellar ataxia type 1 (SCA1) is an adult-onset neurodegenerative disease caused by (CAG) expansion within the coding region of the *ataxin-1 (ATXN1)* gene. In healthy individuals, the (CAG) repeat tract comprises 6–42 repeats interspersed with one to three CAT interruptions. In SCA1 patients, a pure (CAG) expansion of greater than 40 repeats causes disease through toxic protein gain-of-function that is compounded by partial ATXN1 loss-of-function induced by nuclear aggregation and altered protein complex preference.^{1–4} Despite ubiquitous ATXN1 expression, neurodegeneration occurs primarily in cerebellar Purkinje cells (PCs) and brainstem nuclei. This pattern is consistent with clinical symptoms of SCA1 which include gait and limb ataxia, dysarthria, and bulbar dysfunction, among others. To date, there are no disease-modifying therapies for SCA1.

The B05 mouse is a well-characterized model of SCA1. This transgenic line expresses human *ATXN1 (hATXN1)* cDNA containing an 82Q poly-glutamine (polyQ) expansion downstream of the PC promoter, *Pcp2*.⁵ B05 mice develop progressive disease with features similar to SCA1 including impaired motor performance and progressive PC loss.^{6,7}

Precedence for SCA1 disease reversal was established using a conditional version of the B05 mouse wherein normal cellular and behavioral phenotypes were restored following cessation of mutant ATXN1 expression.⁸ Since this finding, we have shown the potential for disease reversal in B05 animals by miRNA-mediated knockdown of hATXN1 when delivered by recombinant adeno-associated virus (rAAV) directly to the deep cerebellar nuclei (DCN), either before or after disease onset.^{9,10}

A second therapeutic approach for SCA1 is overexpression of the ATXN1 paralog, ataxin-1-like (ATXN1L). ATXN1L or Boat (brother-of-ataxin-1) shares 33% overall homology with ATXN1, including the conserved ataxin-1/HBP1 (AXH) domain where both ATXN1 and ATXN1L interact with the transcriptional repressor capicua (CIC).¹¹ Gene duplication of *Atxn1l* in a knockin model of SCA1 (SCA1^{154Q/2Q}) reduced neuropathology and behavioral deficits, likely through displacement of mutant ATXN1 from its native complex with CIC, an interaction that drives cerebellar pathology in SCA1.^{12–14} Using the same delivery strategy as with the artificial miRNA, early rAAV-derived expression of hATXN1L prevented disease phenotypes in B05 and SCA1^{154Q/2Q} mice.^{10,15}

Given the known toxic gain- and loss-of-function qualities of SCA1, we hypothesized that combining hATXN1 knockdown with hATXN1L expression would generate a more robust therapy than

Received 15 March 2022; accepted 10 April 2022;
<https://doi.org/10.1016/j.omtm.2022.04.004>.

Correspondence: Beverly L. Davidson, Raymond G. Perelman Center for Cellular and Molecular Therapeutics, The Children's Hospital of Philadelphia, 3501 Civic Center Boulevard, 6400 Colket Translational Research Building, Philadelphia, PA 19104, USA.

E-mail: davidsonbl@chop.edu



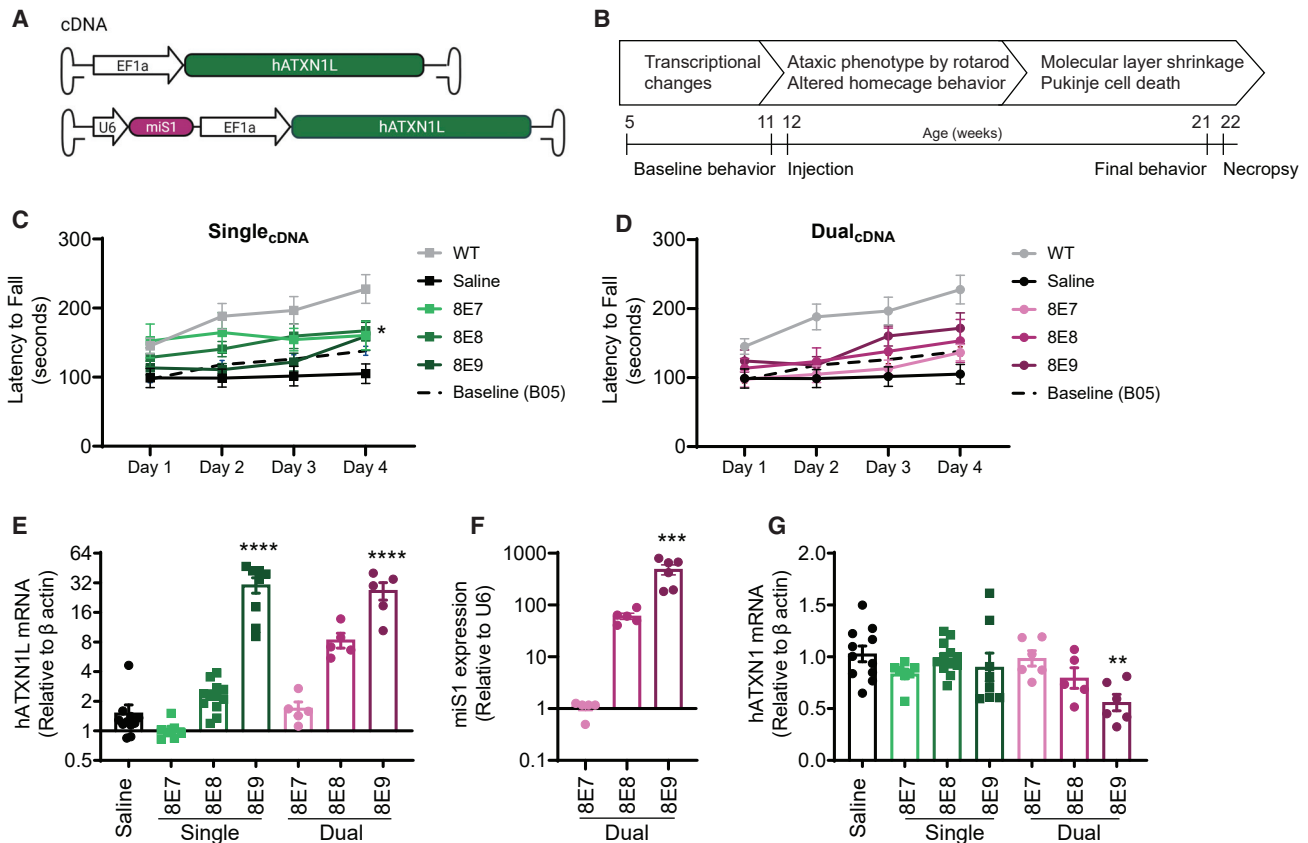


Figure 1. Expression of hATXN1L alone or with miS1 impacts motor phenotype progression in SCA1 mice

(A) Diagram of the Single_{cDNA} (top) and Dual_{cDNA} (bottom) vectors. Dual_{cDNA} contains a separate U6 promoter-driven cassette with the hATXN1L expression cassette. (B) B05 animal disease progression and study timeline. (C) Rotarod performance at 22 weeks for animals treated with Single_{cDNA} vectors (n WT 40, Saline 15, 8E7 14, 8E8 11, 8E9 14). (D) Rotarod performance at 22 weeks for animals treated with Dual_{cDNA} vectors (n WT 40, Saline 15, 8E7 14, 8E8 14, 8E9 14). (E) Measurement of hATXN1L transcripts in total cerebellar RNA. Values are normalized to β actin mRNA and presented relative to saline-injected controls. (F) Mature miS1 expression in cerebella treated with Dual_{cDNA} vectors. Values are normalized to U6 transcripts and plotted relative to the lowest injected dose. (G) Knockdown of hATXN1 mRNA by miS1. Transcripts were normalized to β actin and measured against saline-injected controls. Statistics denote differences from Saline, * $p < 0.05$, ** $p < 0.01$, *** $p < 0.001$, **** $p < 0.0001$. Data represent mean \pm SEM.

overexpression alone.^{10,15} Here, we compared the impact of hATXN1L overexpression alone relative to two dual-expression strategies that combined ATXN1 knockdown and ATXN1L overexpression in a single AAV on SCA1-phenotypes in B05 mice.

RESULTS

Exogenous expression of hATXN1L alone or with miS1 rescues motor phenotype progression in SCA1 animals

Our first dual therapy vector combined separate expression cassettes within a single rAAV and packaged them in AAV5, which like AAV1 gives sufficient PC transduction after DCN delivery to impact B05 disease phenotypes.^{9,15,16} The RNA polymerase III (pol III) promoter U6 was used to drive miS1 expression, the artificial miRNA targeting hATXN1, followed downstream by the cDNA for hATXN1L expressed from the elongation factor 1 alpha (EF1 α) promoter (Dual_{cDNA}; Figure 1A).¹⁵ Efficacy was compared to the EF1 α -hATXN1L

vector, known to prevent disease symptom onset when delivered pre-symptomatically¹⁵ (Single_{cDNA}; Figure 1A).

Disease progression in B05 animals includes a decreased latency to fall from the rotarod by ~ 10 weeks of age compared to wild-type (WT) littermates (Figure 1B).^{6,10} Baseline rotarod assessment at 11 weeks confirmed motor deficits in transgenic B05 animals, and treatment groups were assigned to normalize latency to fall (Figure S1A). At 12 weeks, AAVs harboring either the Single_{cDNA} or Dual_{cDNA} expression cassettes, or saline, were administered bilaterally to the DCN of B05 mice at escalating doses (Table 1). At 9–10 weeks post-injection, animals underwent a final rotarod assessment to measure vector effect.

Single_{cDNA}- or Dual_{cDNA}-treated animals trended toward either no change or an improved latency to fall from the rotarod at 9–10 weeks post-injection compared to baseline (Figures 1C and 1D). In contrast,

Table 1. Study vector dosing

Vector	Dose (vg/mouse)
AAV5/2.Single _{cDNA}	8E7
	8E8
	8E9
AAV5/2.Dual _{cDNA}	8E7
	8E8
	8E9
AAV1/2.Single _{gene}	7.6E7
	7.6E8
	2.7E9
	8E9
	6.5E7
AAV1/2.Dual _{gene}	6.5E8
	2.7E9
	8E9
	8E9

saline-treated animals showed continued progression of disease with decreased latency to fall relative to baseline.

To verify vector processing *in vivo*, RNA was isolated from tissues 1 week following final rotarod assessment. Quantitative real-time PCR (qRT-PCR) on cerebellar RNA showed dose-dependent increases in *hATXN1L* mRNA (Figure 1E). Dual_{cDNA} vector also produced mature miS1 miRNA (Figure 1F) whose expression correlated with decreased *hATXN1* target mRNA levels (Figure 1G).

Dual_{cDNA} vectors reduce inflammatory markers and restore expression of disease-related genes

We next investigated the ability of our therapies to reverse disease-related transcriptomic changes. In B05 animals, glial activation can be detected in B05 mice as early as 4 weeks of age and is attributed to nearby neuronal dysfunction.¹⁷ We previously showed that this phenotype can be exacerbated by excessive AAV-delivered cargo.¹⁰ Transcripts encoding ionized calcium-binding adapter molecule 1 (*Iba1*), a marker of microglial activation, were normalized to levels not statistically different from WT in samples treated with 8E8 and 8E9 vg Dual_{cDNA} vector (Figure S2A), and astrocyte activation, indicated by *Gfap* mRNA levels, did not increase with Dual_{cDNA} treatment (Figure S2B).

Changes in PC-specific transcription have also been well documented.^{18–21} Proper motor coordination requires metabotropic glutamate receptor 1 (mGluR1) expression at PC dendritic spines, and reduced *Grm1* expression has been reported in SCA1 mice.^{8,22} *Grm1* mRNA was partially improved in samples treated with 8E9 vg Dual_{cDNA} (Figure S2C). Mutant ataxin-1 reduces vascular endothelial growth factor A (*Vegfa*) transcripts through repression at the *Vegfa* promoter or post-transcriptionally by miR-150, a miRNA up-regulated in SCA1.^{20,23} *Vegfa* expression in samples from vector-injected mice versus saline-treated mice was not statistically different

from WT (Figure S2D). Taken together, data show that combined *hATXN1L* and miS1 expression when delivered after motor symptom onset improves cell autonomous transcriptional changes and partially restores glial activation.

AAVs expressing *hATXN1L* and miS1 from an engineered minigene improve rotarod phenotypes in B05 mice

As a second approach to combine miS1 with *ATXN1L*, we placed miS1 within an intron upstream of the *hATXN1L*-coding exon. In this manner, both transcripts are driven by the EF1a promoter (Dual_{gene}; Figure 2A).²⁴ To control for potential intron-mediated enhancement of expression,²⁵ the *hATXN1L* vector used for comparison also incorporated the upstream intron (Single_{gene}). Transgenes were packaged in AAV1 and delivered to mice following the same timeline as mentioned earlier (Figure 1B and Table 1).

Consistent with earlier data,²⁴ the transgenes were processed to mature *hATXN1L* mRNA and functional miS1 that reduced *hATXN1* mRNA *in vivo* (Figures 2B–2D). Knockdown of mRNA by rAAV.Dual_{gene} (24%) was less efficient than rAAV.Dual_{cDNA} (35%), consistent with greater miS1 expression when driven by a U6 promoter (Figure S3A), but this difference translated to similar protein knockdown (Figures S3B and S3C). Interestingly, we observed a slight, but significant decrease in *hATXN1* transcripts in mice given 2.7E9 vg rAAV.Single_{cDNA}, which is a phenomenon that has also been observed with presymptomatic delivery of 8E9 vg rAAV.Single_{cDNA}.¹⁵

To estimate relative overexpression of *hATXN1L* compared to endogenous *Atxn1l*, we used a primer/probe set that cross-reacts with the mouse and human sequences. Delivery of the lowest doses increased total *ATXN1L* expression by ~25%, while cerebellar samples from mice given 8E9 vg of rAAV.Dual_{gene} or rAAV.Single_{gene} vectors had 150%–300% overexpression of the human variant (Figure S3D). Similar magnitudes were observed in samples treated with rAAV.Dual_{cDNA} and rAAV.Single_{cDNA} (Figure S3E).

Saline, rAAV.Dual_{gene}, or rAAV.Single_{gene} were injected into the DCN of B05 animals that were previously assessed on the rotarod and showed similar early deficits. 9–10 weeks later, rotarod assays were repeated. Saline-treated animals fell off the rotarod earlier as before, while all Single_{gene}- and Dual_{gene}-vector-treated groups showed significant improvement (Figures 2E and 2F).

miS1 potentiates restoration of dysregulated gene expression over *hATXN1L* alone

To ascertain differences between the Dual versus Single therapy strategies, and whether a multiple or single transcript design was superior, we performed transcriptomic analysis on cerebellar RNA. Samples were isolated from WT and B05 animals injected with saline, 8E9 Single_{cDNA}, and Dual_{cDNA} as well as 8E9 Single_{gene} and Dual_{gene} vectors. Principal component analysis showed clear separation between the B05 saline and WT samples and clustering of biological replicates by treatment group (Figure S4A).

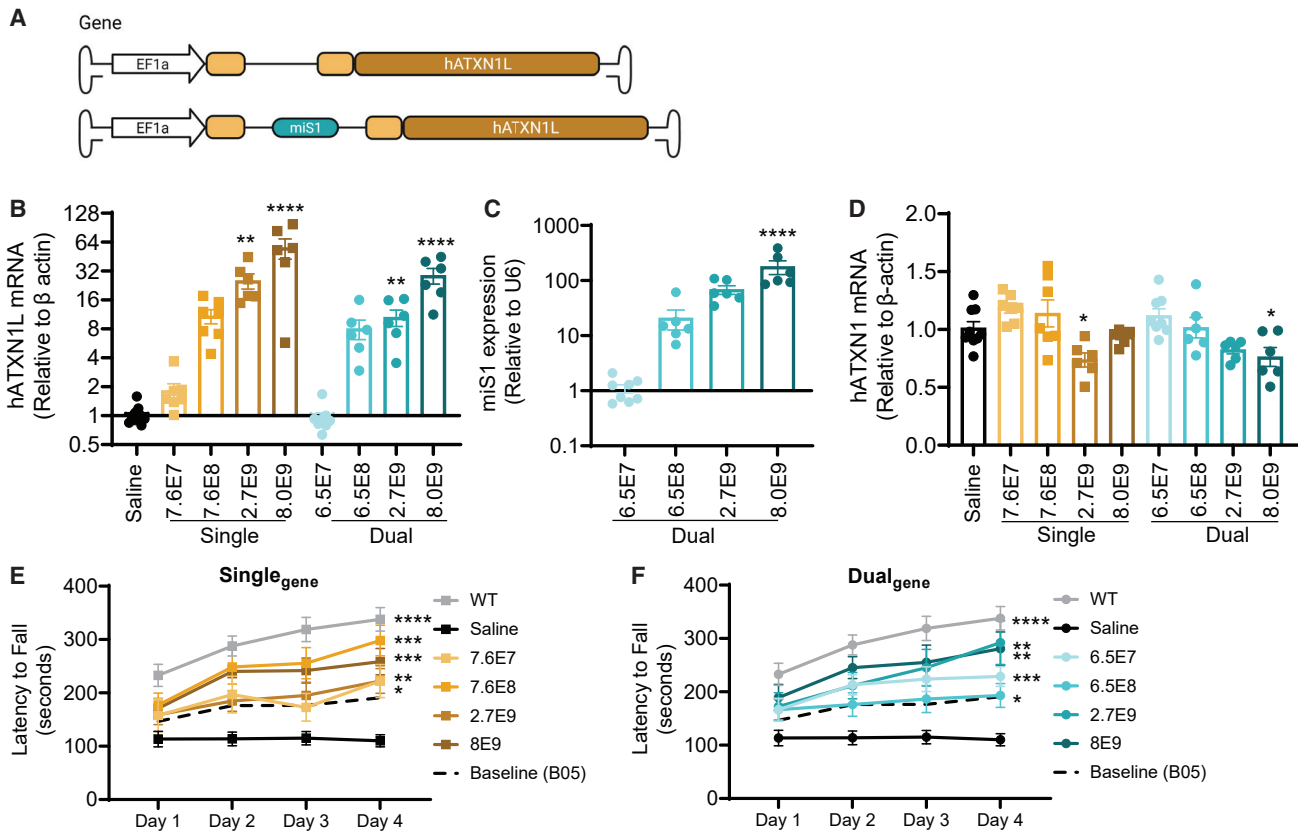


Figure 2. miS1 and hATXN1L processed from a single transcript rescue behavioral decline in B05 animals

(A) Diagram of *Single_{gene}* (top) and *Dual_{gene}* (bottom) vectors. The *Single_{gene}* expresses an ATXN1L minigene from the EF1a promoter. In the *Dual* setting, both hATXN1L and miS1 are driven by EF1a promoter with miS1 processed from within the 5' intron. (B) Quantitative PCR measurement of hATXN1L transcripts in whole cerebellar samples from mice treated with escalating doses of Gene vectors. All samples were normalized to β actin and are presented relative to saline-injected controls. (C) Relative mature miS1 expression in *Dual_{gene}* cerebella. Statistics compare with 6.5E7 vg dose. (D) Quantification of hATXN1 transcripts in Gene treated cerebella. (E) Rotarod performance at 22 weeks (9–10 weeks post-treatment) by animals treated with *Single_{gene}* vectors (n WT 37, Saline 18, 7.6E7 7, 7.6E8 8, 2.7E9 11, 8E9 11). (F) Rotarod performance at 22 weeks by animals treated with *Dual_{gene}* vectors (n WT 37, Saline 18, 6.5E7 9, 6.5E8 8, 2.7E9 11, 8E9 10). Statistics denote differences from Saline on day 4, * $p < 0.05$, ** $p < 0.01$, *** $p < 0.001$, **** $p < 0.0001$. Data represent mean \pm SEM.

Differential gene expression analysis via DESeq2 showed marked gene expression changes between 22-week-old B05-saline-treated animals and WT controls (498 genes, FDR-adjusted p value [pAdj] < 0.05 , $|\log_2$ fold change [\log_2 FC]| ≥ 0.5 ; Figures S4B and S4C, Table S1), with top differentially expressed genes (DEGs) and gene ontology (GO) categorization corresponding to known SCA1 disease genes and pathways (Figures S4D and S4E).^{18,19,21,26}

The broad effect of hATXN1L overexpression is summarized in a heatmap of the top 200 DEGs between WT and saline-treated B05 mice (Figure 3A). Hierarchical clustering demonstrates a stronger effect on gene normalization by rAAV.*Single_{cDNA}* vector compared with rAAV.*Single_{gene}* despite similar hATXN1L transcript levels (Figures 3A, S3D, and S3E). Delivery of rAAV.*Single_{cDNA}* led to a significant change in expression of 292 genes, 101 up- and 191 downregulated compared to B05 saline-treated samples

(Figures 3B and 3C). Quantification of gene correction using our previously defined \log_2 fold change cutoff of 0.5 revealed that 24 of the top 200 DEGs were no longer significantly different from WT following treatment with rAAV.*Single_{cDNA}* (Table S3). In contrast, only the vector-derived hATXN1L transgene was significantly upregulated in *Single_{gene}* samples (\log_2 FC = 6.8329, pAdj = 1.1158e-08). Among the top 20 DEGs in response to hATXN1L overexpression were *Cck*, a prohormone-encoding gene reported to protect against progressive PC atrophy and death in SCA1,^{18,27} and numerous immunoglobulin heavy and light chains, consistent with reactivity of brain-resident B cells to the novel human-based transgene (Table S2).²⁸ Comprehensive transcriptomic analysis in B05 animals has identified a module of genes (the magenta module) that are highly associated with ataxia, enriched in PCs, and rely on ATXN1 as an upstream regulator.¹⁸ Among the 292 genes modified by rAAV.*Single_{cDNA}*, only five were among genes in this module, and none overlapped with key

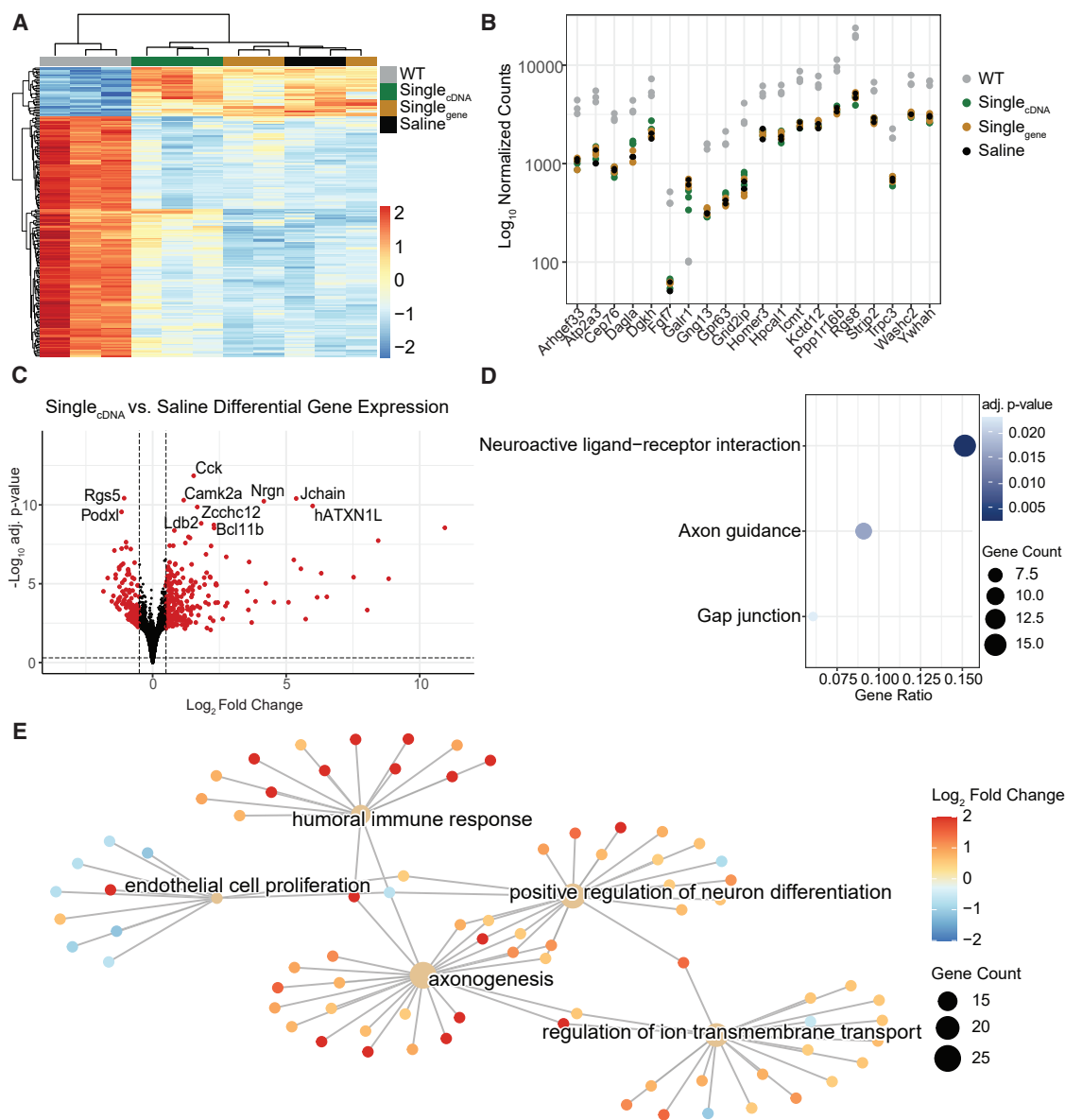


Figure 3. Overexpression of hATXN1L modifies the B05 transcriptome

(A) Heatmap demonstrating the effects of hATXN1L overexpression on the top 200 differentially expressed genes (DEGs) between WT and saline-injected B05 animals. Individual animals are represented, n = 2–3/group, all samples were obtained from male mice. (B) Normalized read counts of the top 20 DEGs in B05 mice following treatment with Single_{cDNA} or Single_{gene} vectors. (C) Volcano plot of the 292 genes differentially expressed following rAAV.Single_{cDNA} delivery. Gene names indicate the top 10 DEGs sorted by pAdj. (D) KEGG pathways associated with rAAV.Single_{cDNA}-dependent genes. (E) Biological process GO terms and categorized genes differentially expressed following treatment with rAAV.Single_{cDNA}.

“hub” genes that exhibit high module connectivity (Figures S5A–S5C).

KEGG pathways enriched among DEGs included neuroactive ligand-receptor interaction and axon guidance (Figure 3D). Consistently, GO analysis identified nervous system development and cell-cell signaling as biological pathways upregulated in

response to hATXN1L overexpression, while genes involved in angiogenesis were downregulated (Figure 3E).

A more robust shift away from the B05 gene expression profile toward WT following Dual_{gene} or Dual_{cDNA} vector treatment is demonstrated in a heatmap of the top 200 DEGs in disease and is summarized in Table 2 (Figure 4A). Among these genes, 88 were normalized to levels

Table 2. Summary of vector-induced gene expression changes

Log ₂ fold change	≥0.5	≤−0.5
Single _{gene} versus Saline	1	0
Single _{cDNA} versus Saline	101	191
Dual _{gene} versus Saline	2	3
Dual _{cDNA} versus Saline	141	114

adjusted p value <0.05

not different from WT in samples ($|\log_2FC| < 0.5$) treated with 8E9 vg Dual_{cDNA} vector and included all 24 genes normalized by Single_{cDNA} (Table S5). Treatment with both Dual_{cDNA} and Dual_{gene} vectors restored expression of the top 20 dysregulated genes in B05 animals toward WT, with stronger effects from Dual_{cDNA} (Figure 4B). As observed for Single_{gene} or Single_{cDNA} vectors, there were a greater number of DEGs in samples treated with Dual_{cDNA} (255 DEGs, $p_{Adj} < 0.05$, $|\log_2FC| \geq 0.5$; Table S4) than Dual_{gene} (5 DEGs; Tables S6 and S7) when compared with saline controls. Among the top 20 genes normalized in response to Dual_{cDNA} vector treatment, eight overlap with the top 20 DEGs in B05 saline animals (Figure 4B). Of the 255 DEGs in response to Dual_{cDNA} treatment, 49 are categorized as downstream effectors of ATXN1 and include all high-connectivity hub genes¹⁸ (Figures 4C, S5D, and S5E).

Functional enrichment categorized using both KEGG and GO biological pathway annotations identified genes involved in calcium signaling pathways, glutamatergic synapses, and synaptic function as overrepresented in response to Dual_{cDNA} vector treatment (Figures 4D and 4E). Humoral immune response, categorized by the observed upregulation of immunoglobulin genes, was identified in Dual_{cDNA} vector-treated samples as was found for Single_{cDNA} (Figures 3E and 4E).

DISCUSSION

We previously demonstrated that AAV vectors encoding *hATXN1*-targeting miRNA can prevent and reverse disease phenotypes in SCA1 mice.^{9,10,15} We have also shown that overexpression of the ATXN1 homolog, ATXN1L, can prevent disease phenotypes when delivered pre-symptomatically.¹⁵ We show that a combination of mutATXN1 knockdown and hATXN1L overexpression generates a more robust therapy than overexpression alone by addressing the gain- and loss-of-function mechanisms of disease.

As functional behavioral outcomes and tissue normalization are important indicators of disease reversal, our prior studies using rAAV-delivered miS1 and hATXN1L focused on these high-level outputs to inform therapeutic efficacy. Here, transcriptomic analysis was performed on treated cerebella to elucidate molecular mechanisms impacted by single or combination therapies. Data was compared with prior results from B05⁵ and ATXN182Q¹³ mouse lines, with confirmed improvement of key disease-related genes. These include *Homer3*, *Atp2a2*, *Rgs8*, *Cck*, *Calb1*, *Pcp2*, and *Grm1*, among others (Table S1).

Incorporation of mutATXN1 into native CIC transcription repressor complexes has been reported as the primary driver of cerebellar pathology in SCA1,¹³ and moderate *Atxn1l* overexpression presumably displaces mutAtxn1 from these same complexes.¹² As such, we anticipated that expression of hATXN1L by rAAV would rescue disease-related gene expression changes. Interestingly, the prior reported transcripts accounted for only 10 of 292 significant DEGs between saline and Single_{cDNA} vector-treated samples (Table S2). More striking, we observed no differential gene expression between Single_{gene} vector and saline-treated samples. Using qPCR and RNAseq counts, we verified similar transgene expression levels in bulk cerebellum and hypothesize that this difference is due to specific cell targeting by the different packaging capsids (AAV1 versus AAV5). Despite limited gene correction, we did observe stabilization or improved motor deficits of B05 mice injected with Single_{cDNA} vector (Figure 1C). Furthermore, mice injected with rAAV.Single_{gene} performed significantly better in a rotarod assay than saline-treated controls, with some groups showing no statistical difference from WT littermates (Figure 3E). We envision two plausible explanations for these results: one is that subtle, non-disease-related gene expression changes function to improve cerebellar health through previously uncharacterized mechanisms, and the other posits that normalization of a few key genes is sufficient to rescue motor phenotypes in B05 mice.

GO characterization of transcripts upregulated by rAAV.Single_{cDNA} identified genes involved in neuron and nervous system development including cell adhesion (*Cntn5*, *Dscam*, and *Thy1*) and signaling molecules (*Dbi*, *Grip2*, *Grm5*, *Gfra1*, and *Shc3*) as well as a cluster of genes involved in synaptic transmission (Figure 3E). Interestingly, most of these genes (61/91) contain motifs for the transcription factor zinc finger of the cerebellum 1 (*Zic1*), a transcription factor required for appropriate cerebellar development.²⁹ Taken together, these data support a pattern of cerebellar restoration by ATXN1L.

In samples from animals treated with Single_{cDNA} vector, we identified four genes (*Cck*, *Camk2a*, *Bcl11a*, and *Cntnap5c*) that showed significant differences compared with saline controls and were not statistically different from WT. *Cck* is primarily expressed in PCs of the adult cerebellum and shows strong downregulation in SCA1 and SCA2 mouse models.^{18,30} Overexpression of *Cck* protects against PC toxicity in a mouse model of severe ataxia through activation of the *Cck* receptor, *Cck1r*.¹⁸ Recently, Wozniak, et al. corroborated this result, showing that direct activation of *Cck1r* by the agonist A71623 reduces PC pathology and motor phenotypes in B05 animals, as well as a repeat expansion model of SCA2.²⁷ Mechanistically these improvements were attributed to normalization of mTORC1 signaling, disruption of which has been shown to alter synaptic function and cell morphology.^{31–35} Our analysis did not reveal overlap between disease-related and known mTORC1-target genes,^{36,37} and only one known target, *Timp2*, was increased by rAAV.Single_{cDNA} delivery. Direct comparison with *Cck1R* agonist-treated samples may reveal a *Cck*-dependent mechanism of action by hATXN1L overexpression.

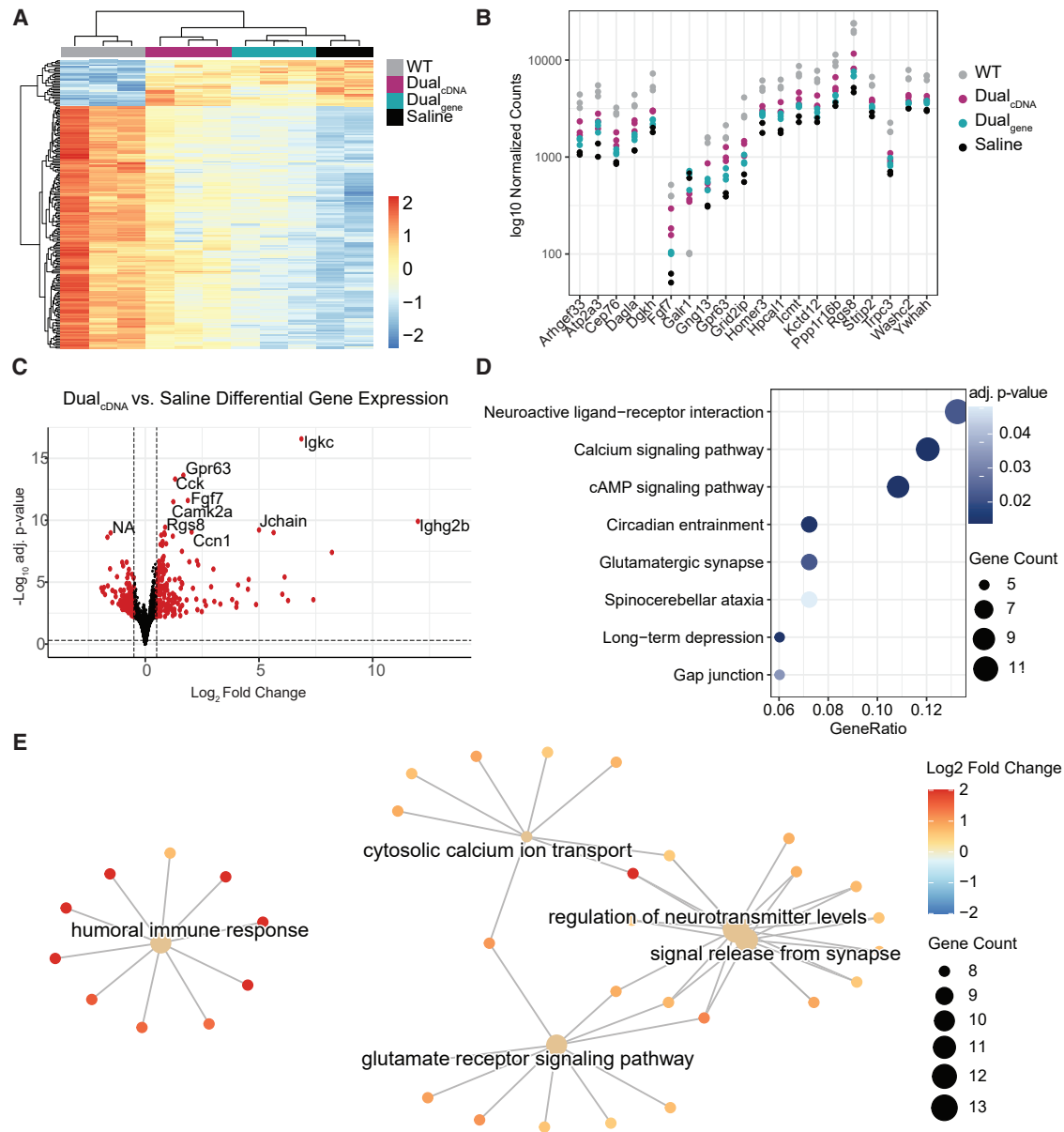


Figure 4. rAAV.Dual vectors normalize expression of key SCA1 genes and pathways

(A) Heatmap demonstrating the effects of rAAV.Dual vector delivery on the top 200 DEGs between WT and saline-injected B05 animals. Individual animals are represented, $n = 2-3$ /group, and all samples were obtained from male mice. (B) Normalized read counts of the top 20 DEGs in B05 mice following injection with Dual_{cDNA} and Dual_{gene} vectors. (C) Volcano plot of the 255 genes differentially expressed following rAAV.Single_{cDNA} delivery. Gene names indicate the top 10 DEGs sorted by pAdj. (D) KEGG pathways affected by rAAV.Dual_{cDNA} delivery. (E) Cluster diagrams depicting biological process GO terms and associated genes following treatment with rAAV.Dual_{cDNA}.

Prior work supporting functionally redundant roles for ATXN1 and ATXN1L has used the SCA1^{154Q} knockin model.^{2,12} Different from the B05 mouse model used in this study, SCA1^{154Q} mice express repeat-expanded ATXN1L from the endogenous locus at endogenous levels.¹⁴ It is possible that overexpression of hATXN1L alone is insufficient to compete with the 30 mutATXN1 transgene copies in B05 mice.⁵ Consistent with this hypothesis, we show that delivery of rAAV.Dual_{cDNA} robustly normalizes disease-related transcripts,

including genes whose expression changes have been attributed to ATXN1 loss of function based on their common misregulation in ATXN1^{-/-} and SCA1^{154Q/2Q} mice (*Atp2a3*, *Igf1*, *Ngef*, *Homer3*, among others; Table S4).² Furthermore, rather than an additive effect, we observed a shift in gene targets when *mutATXN1* transcripts were reduced by miS1 (Tables S2 and S4) with only 84 of 292 DEGs by Single_{cDNA} vector also significantly changed by Dual_{cDNA}. This supports a gain of function by overexpressed hATXN1L that is

neuroprotective but does not function through the expected ATXN1-CIC axis. Future experiments in SCA1^{154Q} animals would allow us to measure outcomes of virally delivered hATXN1L in a setting of physiological ATXN1L expression.

Delivery of rAAVs expressing either hATXN1L or miS1 to B05 mice prior to symptom onset equally normalizes rotarod performance after 32 weeks to levels not different from WT controls.¹⁵ At 11 weeks post-injection, we did not find a significant difference by rotarod assay between mice given similar doses of Single or Dual vectors within their respective studies, supporting a common mechanism of action between the two therapies. Among the 84 shared DEGs following treatment with both Single_{cDNA} and Dual_{cDNA} vectors, 38 were categorized in nervous system development and synaptic transmission and included Cck.

Although not evident from the behavior studies, transcriptomic analysis showed that addition of miS1 is advantageous for disease reversal in B05 mice, normalizing mutATXN1-dependent gene expression, including many with promoter-localized CIC binding motifs (Figure 4).¹⁸ Like Single vector-treated animals, only rAAV. Dual_{cDNA}-injected animals showed statistically significant gene expression changes, with sub-threshold changes detected in rAAV. Dual_{gene} samples (Tables S4 and S6). In addition to distinct packaging capsids, this result may reflect differences in mutATXN1 knockdown by mature miS1 arising from RNA pol III transcripts versus an RNA pol II transcript intron (Figures 1A, 1G, 3A, 3D, and S3A). Given our extensive prior characterization of AAV-delivered miS1,^{9,10,15,24,38} we did not include an rAAV.miS1 cohort in our current study. While RNA sequencing of samples from animals treated with rAAV.miS1 would allow us to discriminate therapeutic effects of mutATXN1 knockdown, our most recent work in non-human primates supports inclusion of a strong RNA pol II promoter for long-term vector safety.²⁴

In summary, we show that overexpression of hATXN1L is sufficient to stabilize or reverse behavioral deficits following symptom onset in B05 mice, and broad, disease-specific gene normalization requires concomitant knockdown of mutATXN1 by miS1. Mechanistically, we propose that this represents an inability of hATXN1L to fully compete with established toxicity by high levels of mutATXN1, a situation that may not be encountered in a setting of genetic *Atxn1l* duplication or presymptomatic rAAV delivery. Our data support combination of both therapeutic strategies into a single rAAV for efficient delivery of a vector capable of overcoming both loss- and gain-of-function mechanisms of disease in SCA1.

MATERIALS AND METHODS

Plasmids and viral vectors

The therapeutic miRNA sequence targeting human and rhesus Ataxin-1 (miS1) and the overexpression construct of *ATXN1L* (Single_{cDNA}) have been described.^{10,15} The proviral plasmid used to generate our Dual_{cDNA} virus was generated by ligating the U6 promoter and miS1 at an EcoRI restriction site upstream the elon-

gation factor 1-alpha (EF1a) promoter. Minigene proviral plasmids were also adapted from our hATXN1L construct and modified as described previously.²⁴ Briefly, two *Atxn1l* genomic segments (hg38, chr16:71848010-71848392 and chr16:71849295-71850155) were amplified from HEK293 DNA with NEB HiFi Assembly compatible primers that incorporated a short linker (BstBI-NheI-BmtI-MluI) between the segments. miS1, including the entire modified miR-30 scaffold and short (~40 bp) flanking sequence, was ligated into the intronic linker at NheI and MluI sites.

Recombinant AAV serotype AAV2/5 (cDNA) or AAV2/1 (Gene) vectors were generated at the Children's Hospital of Philadelphia Research Vector Core and resuspended in Diluent Buffer (Research Vector Core). Vector titers were determined by quantitative PCR using primers targeting the hATXN1L transgene (Hs04964302_s1, Thermo Fisher).

Animals

All animal protocols were approved by the Children's Hospital of Philadelphia Animal Use and Care Committee. B05 mice were developed by Dr. H. T. Orr at the University of Minnesota⁵ and were re-derived by Jackson Laboratories in 2014 and are maintained on a pure FVB background. All study animals were obtained from litters derived from breeding hemizygous positive B05 males with WT FVB females from Jackson Laboratories (Bar Harbor, ME). Genotypes were determined by PCR for the mutant transgene.⁵ All study groups are age matched and include approximately equal numbers of male and female mice. Animals were housed in a climate-controlled environment and kept on a 12-hr light/dark cycle with access to food *ad libitum*.

AAV injection and tissue isolation

At 12 weeks of age, B05 mice were injected bilaterally into the DCN (coordinates: -6.0 mm caudal to bregma, ±2 mm from the midline, and -2.2 mm deep from the cerebellar surface) with rAAV vectors expressing hATXN1L alone (Single) or hATXN1L and miS1 (Dual). Viruses or saline (Diluent buffer) were delivered in 4 µL volume/hemisphere at doses outlined in Table 1. At 22 weeks of age, mice were anesthetized with 2.5% isoflurane/oxygen mixtures and transcardially perfused with ice-cold saline. Cerebellar hemispheres for histological analyses were post-fixed overnight in 4% paraformaldehyde before transferring to 30% sucrose solution for 48 h. Hemispheres were then embedded in Cryo OCT Compound (Thermo Fisher) medium, frozen in a dry-ice chilled ethanol bath and stored at -80°C until sectioning. Hemispheres for RNA were transferred to 1 mL TRIzol (Invitrogen) and snap frozen in liquid nitrogen followed by storage at -80°C. Samples for all other analyses were snap frozen in liquid nitrogen and stored at -80°C until use.

RNA isolation and quantification

RNA was isolated using TRIzol according to manufacturer's instructions (Invitrogen). RNA samples were DNase-treated with TURBO DNA-free kit (Invitrogen) and reverse transcribed using MultiScribe Reverse Transcriptase (Applied Biosystems) with Random

Hexamers for mRNA quantification, stem-loop primers for miRNA quantification (miS1 – 5'- GTC GTA TCC AGT GCA GGG TCC GAG GTA TTC GCA CTG GAT ACG ACA GCA AC, U6- TAT GGA ACG CTT CAC GAA TTT G), and a transgene-specific primer localized to the BGH polyA region to assess transgene splicing (5'- ACA GTG GGA GTG GCA CCT TC). qRT-PCR measurements were made using a CFX384 Real Time System from Bio-Rad on samples prepared using TaqMan Universal Master Mix II, no UNG (Applied Biosystems) with TaqMan primer/probe sets directed against hATXN1 (Hs00165656_m1), hATXN1L (Hs04964302_s1), mIba1 (Mm00479862_g1), mGFAP (Mm01253033_m1), and mouse β -actin (4352341E). miS1 levels were quantified using Fwd 5' GTG CAGGGTCCGAGGTATT and Probe: /56-FAM/CACTGGATA/ZEN/CGACGAGCAACGA/3IABkFQ and U6 using Fwd 5' GCT TCG GCA GCA CAT AT ACT A and Rev 5' CGA ATT TGC GTG TCA TCC TTG and Probe: /56-FAM/ACGATACAG/ZEN/AGAAG ATTAGCATGGCCC/3IABkFQ/.

RNAseq library preparation and sequencing

Total RNA (1 μ g) was extracted from tissue using TRIzol (Invitrogen) and treated to remove contaminating DNA using RNAeasy Plus Miniprep kit (QIAGEN). RIN values were acquired using RNA Nano Chips (Agilent Technologies) in Agilent 2100 BioAnalyzer per manufacturer's protocol. Sequencing libraries were prepared using NEBNext Ultra II Directional RNA Library Prep Kit for Illumina (New England Biolabs). rRNA depletion was performed using combined human, mouse, and rat species-specific QIAseq FastSelect RNA Removal Kit (QIAGEN). SPRiselect Beads (Beckman Coulter) were used for the purification steps. cDNA libraries were then indexed using the NEBNext Dual Index Kit (New England Biolabs). Samples were analyzed on High Sensitivity DNA Chips (Agilent Technologies) with Agilent 2100 BioAnalyzer per manufacturer's protocol to determine library size, concentration, and purity. Libraries were indexed and pooled at concentrations of 1 nM, then run on a NovaSeq 6000 S1 flow cell (Illumina) using NovaSeq Control Software v1.5. The resulting sequencing reads, in fastq format, were aligned to the Mus Musculus genome (GRCm39.104) obtained from ensembl.org. Alignment was performed with the STAR (STAR_2.6.0c) aligner.³⁹ Read counts-per-gene values generated by STAR were used as the basis for differential expression analysis performed using DESeq2 version 1.20.1 (R version 3.6.1).⁴⁰ clusterProfiler (version 4.1.4)⁴¹ was used for all functional enrichment analyses. Data visualization was also performed in R and associated modalities within EnhancedVolcano (version 1.9.11), tidyverse (version 1.3.1), dbplyr (version 2.1.1), ggplot2 (version 3.3.5), pheatmap (version 1.0.12), and RColorBrewer (version 1.1.2).

Western blot analysis

Individual cerebellar hemispheres were homogenized in 400 μ L RIPA buffer (50 mM Tris-HCl, pH 8, 150 mM NaCl, 1% IGEPAL CA-630, 0.5% sodium deoxycholate, 0.1% SDS) supplemented with 1x cOmplete Protease Inhibitors (Roche). Samples were incubated on ice for 30 min then spun at $>18,000 \times g$ for 20 min at 4°C. Supernatant protein concentration was measured using a DC Protein Assay Kit

(Bio-Rad). Five micrograms were loaded into 4%–12% Criterion XT Bis-Tris gels (Bio-Rad) and transferred to PVDF membranes for blotting. Membranes were blocked for 1 h at RT in 5% milk in 1x TBST (137 mM NaCl, 2.7 mM KCl, 19 mM Tris Base, 0.1% Tween-20). Rabbit anti-ATXN1 11NQ was diluted 1:2000 in 2% BSA in TBST and incubated overnight (O/N) at 4°C followed by goat anti-rabbit IgG HRP (Thermo Fisher) diluted 1:10,000 in 5% milk in TBST. Membranes were exposed using ECL Prime Western Blotting Detection Reagent (Cytiva). Without stripping, blots were re-probed using mouse anti-alpha tubulin Clone B-5-1-2 (Thermo Fisher) diluted 1:10,000 in 5% milk TBST O/N at 4°C followed by secondary goat anti-mouse IgG HRP (Thermo Fisher) 1:10,000 in 5% milk.

Rotarod analysis

Baseline testing was conducted at 11 weeks of age, prior to intervention, and then again before sacrifice at 22 weeks. On day 1, mice were habituated to the Rotarod for 5 min with rotation at 5 rpm. Mice were then tested in three trials per day, separated by a minimum of 30 min, for four consecutive days. The protocol consisted of acceleration from 4 to 40 rpm over 4 (fast-ramp) or 5 (slow-ramp) minutes followed by a hold at 40 rpm for a maximum run time of 500 s. Latency to fall was recorded as the time when mice fell from the rod or held on for two consecutive rotations without running. Mice still on at the end of the protocol were removed manually and recorded as 500 s. Initial Rotarod results were used to distribute B05 mice among treatment groups. Two-way ANOVA (trial day and treatment) followed by Bonferroni post-hoc analysis was used to assess statistical differences.

SUPPLEMENTAL INFORMATION

Supplemental information can be found online at <https://doi.org/10.1016/j.omtm.2022.04.004>.

ACKNOWLEDGMENTS

This work was funded by the NIH NS094355 (M.S.K. and B.L.D.), the National Ataxia Foundation (B.L.D and M.S.K), and the Children's Hospital of Philadelphia Research Institute. Graphical abstract was created with BioRender.com.

AUTHOR CONTRIBUTIONS

E.M.C., M.S.K., and A.B.R. designed and performed experiments, evaluated the data, and wrote and edited the manuscript. B.L.D. designed the study, evaluated the data, and wrote and edited the manuscript.

DECLARATION OF INTERESTS

B.L.D. is a founder of Spark Therapeutics and Spirovant Sciences. She serves an advisory role and/or receives sponsored research support for her laboratory from Roche, Novartis, Homology Medicines, Resilience, Spirovant Sciences, Saliogen, Patch Bio, Panorama Medicines, and Voyager Therapeutics.

REFERENCES

- Lim, J., Crespo-Barreto, J., Jafar-Nejad, P., Bowman, A.B., Richman, R., Hill, D.E., Orr, H.T., and Zoghbi, H.Y. (2008). Opposing effects of polyglutamine expansion on native protein complexes contribute to SCA1. *Nature* 452, 713–718.
- Crespo-Barreto, J., Fryer, J.D., Shaw, C.A., Orr, H.T., and Zoghbi, H.Y. (2010). Partial loss of ataxin-1 function contributes to transcriptional dysregulation in spinocerebellar ataxia type 1 pathogenesis. *PLoS Genet.* 6, e1001021.
- Duyckaerts, C., Durr, A., Cancel, G., and Brice, A. (1999). Nuclear inclusions in spinocerebellar ataxia type 1. *Acta Neuropathol.* 97, 201–207.
- Skinner, P.J., Koshy, B.T., Cummings, C.J., Klement, I.A., Helin, K., Servadio, A., Zoghbi, H.Y., and Orr, H.T. (1997). Ataxin-1 with an expanded glutamine tract alters nuclear matrix-associated structures. *Nature* 389, 971–974.
- Burright, E.N., Clark, H.B., Servadio, A., Matilla, T., Feddersen, R.M., Yunis, W.S., Duvick, L.A., Zoghbi, H.Y., and Orr, H.T. (1995). SCA1 transgenic mice: a model for neurodegeneration caused by an expanded CAG trinucleotide repeat. *Cell* 82, 937–948.
- Clark, H.B., Burright, E.N., Yunis, W.S., Larson, S., Wilcox, C., Hartman, B., Matilla, A., Zoghbi, H.Y., and Orr, H.T. (1997). Purkinje cell expression of a mutant allele of SCA1 in transgenic mice leads to disparate effects on motor behaviors, followed by a progressive cerebellar dysfunction and histological alterations. *J. Neurosci.* 17, 7385–7395.
- Robitaille, Y., Lopes-Cendes, I., Becher, M., Rouleau, G., and Clark, A.W. (1997). The neuropathology of CAG repeat diseases: review and update of genetic and molecular features. *Brain Pathol.* 7, 901–926.
- Zu, T., Duvick, L.A., Kaytor, M.D., Berlinger, M.S., Zoghbi, H.Y., Clark, H.B., and Orr, H.T. (2004). Recovery from polyglutamine-induced neurodegeneration in conditional SCA1 transgenic mice. *J. Neurosci.* 24, 8853–8861.
- Keiser, M.S., Boudreau, R.L., and Davidson, B.L. (2014). Broad therapeutic benefit after RNAi expression vector delivery to deep cerebellar nuclei: implications for spinocerebellar ataxia type 1 therapy. *Mol. Ther.* 22, 588–595.
- Keiser, M.S., Monteys, A.M., Corbau, R., Gonzalez-Alegre, P., and Davidson, B.L. (2016). RNAi prevents and reverses phenotypes induced by mutant human ataxin-1. *Ann. Neurol.* 80, 754–765.
- Mizutani, A., Wang, L., Rajan, H., Vig, P.J., Alaynick, W.A., Thaler, J.P., and Tsai, C.C. (2005). Boat, an AXH domain protein, suppresses the cytotoxicity of mutant ataxin-1. *EMBO J.* 24, 3339–3351.
- Bowman, A.B., Lam, Y.C., Jafar-Nejad, P., Chen, H.K., Richman, R., Samaco, R.C., Fryer, J.D., Kahle, J.J., Orr, H.T., and Zoghbi, H.Y. (2007). Duplication of Atxn1l suppresses SCA1 neuropathology by decreasing incorporation of polyglutamine-expanded ataxin-1 into native complexes. *Nat. Genet.* 39, 373–379.
- Rousseaux, M.W.C., Tschumperlin, T., Lu, H.C., Lackey, E.P., Bondar, V.V., Wan, Y.W., Tan, Q., Adamski, C.J., Friedrich, J., Twaroski, K., et al. (2018). ATXN1-C1C complex is the primary driver of cerebellar pathology in spinocerebellar ataxia type 1 through a gain-of-function mechanism. *Neuron* 97, 1235–1243.e5.
- Watake, K., Weeber, E.J., Xu, B., Antalffy, B., Yuva-Paylor, L., Hashimoto, K., Kano, M., Atkinson, R., Sun, Y., Armstrong, D.L., et al. (2002). A long CAG repeat in the mouse Sca1 locus replicates SCA1 features and reveals the impact of protein solubility on selective neurodegeneration. *Neuron* 34, 905–919.
- Keiser, M.S., Geoghegan, J.C., Boudreau, R.L., Lennox, K.A., and Davidson, B.L. (2013). RNAi or overexpression: alternative therapies for Spinocerebellar Ataxia Type 1. *Neurobiol. Dis.* 56, 6–13.
- Boudreau, R.L., Martins, I., and Davidson, B.L. (2009). Artificial microRNAs as siRNA shuttles: improved safety as compared to shRNAs in vitro and in vivo. *Mol. Ther.* 17, 169–175.
- Cvetanovic, M., Ingram, M., Orr, H., and Opal, P. (2015). Early activation of microglia and astrocytes in mouse models of spinocerebellar ataxia type 1. *Neuroscience* 289, 289–299.
- Ingram, M., Wozniak, E.A.L., Duvick, L., Yang, R., Bergmann, P., Carson, R., O'Callaghan, B., Zoghbi, H.Y., Henzler, C., and Orr, H.T. (2016). Cerebellar transcriptome profiles of ATXN1 transgenic mice reveal SCA1 disease progression and protection pathways. *Neuron* 89, 1194–1207.
- Serra, H.G., Byam, C.E., Lande, J.D., Tousey, S.K., Zoghbi, H.Y., and Orr, H.T. (2004). Gene profiling links SCA1 pathophysiology to glutamate signaling in Purkinje cells of transgenic mice. *Hum. Mol. Genet.* 13, 2535–2543.
- Rodriguez-Lebron, E., Liu, G., Keiser, M., Behlke, M.A., and Davidson, B.L. (2013). Altered Purkinje cell miRNA expression and SCA1 pathogenesis. *Neurobiol. Dis.* 54, 456–463.
- Lin, X., Antalffy, B., Kang, D., Orr, H.T., and Zoghbi, H.Y. (2000). Polyglutamine expansion down-regulates specific neuronal genes before pathologic changes in SCA1. *Nat. Neurosci.* 3, 157–163.
- Ichise, T., Kano, M., Hashimoto, K., Yanagihara, D., Nakao, K., Shigemoto, R., Katsuki, M., and Aiba, A. (2000). mGluR1 in cerebellar Purkinje cells essential for long-term depression, synapse elimination, and motor coordination. *Science* 288, 1832–1835.
- Cvetanovic, M., Patel, J.M., Marti, H.H., Kini, A.R., and Opal, P. (2011). Vascular endothelial growth factor ameliorates the ataxic phenotype in a mouse model of spinocerebellar ataxia type 1. *Nat. Med.* 17, 1445–1447.
- Keiser, M.S., Ranum, P.T., Yrigollen, C.M., Carrell, E.M., Smith, G.R., Muehlmann, A.L., Chen, Y.H., Stein, J.M., Wolf, R.L., Radaelli, E., et al. (2021). Toxicity after AAV delivery of RNAi expression constructs into nonhuman primate brain. *Nat. Med.* 27, 1982–1989.
- Palmiter, R.D., Sandgren, E.P., Avarbock, M.R., Allen, D.D., and Brinster, R.L. (1991). Heterologous introns can enhance expression of transgenes in mice. *Proc. Natl. Acad. Sci. U S A* 88, 478–482.
- Gatchel, J.R., Watake, K., Thaller, C., Carson, J.P., Jafar-Nejad, P., Shaw, C., Zu, T., Orr, H.T., and Zoghbi, H.Y. (2008). The insulin-like growth factor pathway is altered in spinocerebellar ataxia type 1 and type 7. *Proc. Natl. Acad. Sci. U S A* 105, 1291–1296.
- Wozniak, E.A.L., Chen, Z., Paul, S., Yang, P., Figueroa, K.P., Friedrich, J., Tschumperlin, T., Berken, M., Ingram, M., Henzler, C., et al. (2021). Cholecystokinin 1 receptor activation restores normal mTORC1 signaling and is protective to Purkinje cells of SCA mice. *Cell Rep.* 37, 109831.
- Knopf, P.M., Harling-Berg, C.J., Cserr, H.F., Basu, D., Sirulnick, E.J., Nolan, S.C., Park, J.T., Keir, G., Thompson, E.J., and Hickey, W.F. (1998). Antigen-dependent intrathecal antibody synthesis in the normal rat brain: tissue entry and local retention of antigen-specific B cells. *J. Immunol.* 161, 692–701.
- Aruga, J., Minowa, O., Yaginuma, H., Kuno, J., Nagai, T., Noda, T., and Mikoshiba, K. (1998). Mouse Zic1 is involved in cerebellar development. *J. Neurosci.* 18, 284–293.
- Pflieger, L.T., Dansithong, W., Paul, S., Scoles, D.R., Figueroa, K.P., Meera, P., Otis, T.S., Facelli, J.C., and Pulst, S.M. (2017). Gene co-expression network analysis for identifying modules and functionally enriched pathways in SCA2. *Hum. Mol. Genet.* 26, 3069–3080.
- Jaworski, J., Spangler, S., Seeburg, D.P., Hoogenraad, C.C., and Sheng, M. (2005). Control of dendritic arborization by the phosphoinositide-3'-kinase-Akt-mammalian target of rapamycin pathway. *J. Neurosci.* 25, 11300–11312.
- Stoica, L., Zhu, P.J., Huang, W., Zhou, H., Kozma, S.C., and Costa-Mattioli, M. (2011). Selective pharmacogenetic inhibition of mammalian target of Rapamycin complex I (mTORC1) blocks long-term synaptic plasticity and memory storage. *Proc. Natl. Acad. Sci. U S A* 108, 3791–3796.
- McCabe, M.P., Cullen, E.R., Barrows, C.M., Shore, A.N., Tooke, K.I., Laprade, K.A., Stafford, J.M., and Weston, M.C. (2020). Genetic inactivation of mTORC1 or mTORC2 in neurons reveals distinct functions in glutamatergic synaptic transmission. *Elife* 9, e51440.
- Henry, F.E., McCartney, A.J., Neely, R., Perez, A.S., Carruthers, C.J., Stuenkel, E.L., Inoki, K., and Sutton, M.A. (2012). Retrograde changes in presynaptic function driven by dendritic mTORC1. *J. Neurosci.* 32, 17128–17142.
- Urbanska, M., Gozdz, A., Swiech, L.J., and Jaworski, J. (2012). Mammalian target of rapamycin complex 1 (mTORC1) and 2 (mTORC2) control the dendritic arbor morphology of hippocampal neurons. *J. Biol. Chem.* 287, 30240–30256.

36. Laplante, M., and Sabatini, D.M. (2013). Regulation of mTORC1 and its impact on gene expression at a glance. *J. Cell Sci.* *126*, 1713–1719.
37. Duvel, K., Yecies, J.L., Menon, S., Raman, P., Lipovsky, A.I., Souza, A.L., Triantafellow, E., Ma, Q., Gorski, R., Cleaver, S., et al. (2010). Activation of a metabolic gene regulatory network downstream of mTOR complex 1. *Mol. Cell* *39*, 171–183.
38. Keiser, M.S., Kordower, J.H., Gonzalez-Alegre, P., and Davidson, B.L. (2015). Broad distribution of ataxin 1 silencing in rhesus cerebella for spinocerebellar ataxia type 1 therapy. *Brain* *138*, 3555–3566.
39. Dobin, A., Davis, C.A., Schlesinger, F., Drenkow, J., Zaleski, C., Jha, S., Batut, P., Chaisson, M., and Gingeras, T.R. (2013). STAR: ultrafast universal RNA-seq aligner. *Bioinformatics* *29*, 15–21.
40. Love, M.I., Huber, W., and Anders, S. (2014). Moderated estimation of fold change and dispersion for RNA-seq data with DESeq2. *Genome Biol.* *15*, 550.
41. Wu, T., Hu, E., Xu, S., Chen, M., Guo, P., Dai, Z., Feng, T., Zhou, L., Tang, W., Zhan, L., et al. (2021). clusterProfiler 4.0: a universal enrichment tool for interpreting omics data. *Innovation* *2*, 100141.